A MIMO Joint Communication-Radar Measurement Platform at the Millimeter-Wave Band

(Invited Paper)

Preeti Kumari[‡], Amine Mezghani[*], Robert W. Heath Jr[‡],
[‡]WNCG, The University of Texas at Austin, TX, US, {preeti_kumari, rheath}@utexas.edu
[*]University of Manitoba, Canada, amine.mezghani@umanitoba.ca

***Abstract*—A fully-digital wideband joint communication-radar (JCR) at the millimeter-wave (mmWave) band will simultaneously enable high communication and radar performances with enhanced design flexibility. In this paper, we present a measurement platform with a software-defined architecture to evaluate and demonstrate the performance of these JCR systems using real channel measurements. We develop this platform by extending a mmWave communication set-up with an additional full-duplex radar receiver and by capturing the MIMO JCR channel using a moving antenna on a sliding rail. To characterize the JCR performance, we conduct indoor experiments and apply traditional/advanced processing algorithms on the measured data. The results demonstrate that our testbed at 73 GHz with 2 GHz bandwidth can capture the JCR channel with high range/direction estimation accuracy. The comparison between the communication and radar channel shows the potential for improving JCR performance by exploiting the antenna diversity due to widely-separated communication and radar receivers.**

***Index Terms*—Millimeter-wave MIMO, joint communication and radar, fully-digital waveform, experimental demonstration**

I. Introduction

A joint communication and radar (JCR) system that uses a common transmit (TX) signal will enable hardware/spectrum reuse with significant benefits in cost, size, and power consumption. To meet the demanding requirements of next-generation applications, such as autonomous driving [1] and smart connected devices [2], a JCR system would need to achieve high data rate communication and high resolution sensing with a wide field-of-view (FoV), and low latency. A millimeter-wave (mmWave) MIMO JCR with a fully digital TX and receive (RX) processing is a solution to simultaneously realize enhanced communication and radar performance with increased design flexibility in terms of waveform and beamforming techniques for futuristic systems.

The prior approaches on mmWave JCR systems are mainly classified as either radar-centric or communication-centric [3]. The radar-centric JCR approach, however, suffers from low data rates because their waveforms spread the communication signal to avoid disturbing the radar properties. In [4]–[7], theoretical frameworks for communication-centric mmWave JCRs were developed by exploiting the preamble of the mmWave WLAN standard for high-resolution radar sensing. The IEEE 802.11ad standard, however, supports mmWave analog beamforming that leads to a large trade-off between communication and radar performances.

Because of hardware limitations, prototyping at mmWave has been difficult, especially for mmWave communications. The recent wideband mmWave communications testbeds either exist at 60 GHz [8], [9] or 71-76 GHz band [10]. Recently, [8] investigated the applicability of the IEEE 802.11ad technology at 60 GHz for communications on a vehicular testbed using Tensorcom 802.11ad module. In [9], the feasibility of IEEE 802.11ad-based radar in the range domain was performed indoors using a Dell laptop with IEEE 802.11ad functionality at 60 GHz. The testbeds developed in [8], [9], however, used analog beamforming and was not fully programmable. Additionally, the strong atmospheric absorption at 60 GHz makes it difficult for future outdoor-to-indoor communications, when compared to 71-76 GHz [11]. The existing mmWave testbeds with software-defined radio architecture and fully digital waveform generation/processing have demonstrated gigabits-per-second communication data rate at 71-76 GHz band [12], [13].

In this paper, we present a MIMO JCR testbed at 71-76 GHz band with 2 GHz bandwidth to demonstrate and evaluate the performance of a communication-centric mmWave JCR. To our knowledge, this is the first wideband MIMO JCR testbed with software-defined architecture and a fully digital waveform generation/processing at 71-76 GHz band. We develop this testbed by extending the National Instruments (NI) mmWave platform for 5G communications [10], [12] to a JCR mmWave testbed with a full-duplex radar receiver with several digital receive channels. To perform MIMO radar characterization of the communication-centric JCR testbed, we conduct experiments using a trihedral corner reflector. We also perform simultaneous joint communication-radar channel measurements to explore the similarities and dissimilarities between the communication and radar channel. We apply traditional as well as advanced receive processing techniques. Our results show the high-resolution channel estimation capability of the JCR system with a wide FoV.

II. Theoretical Background

We consider a mmWave joint communication-radar system, where a full-duplex source transmits a JCR waveform to a communication receiver, while simultaneously receiving echoes from the surrounding targets and clutter, as shown in Fig. 1. Digital beamforming is used on the RX using a b-bit ADC per antenna. We assume the RX antenna array is a

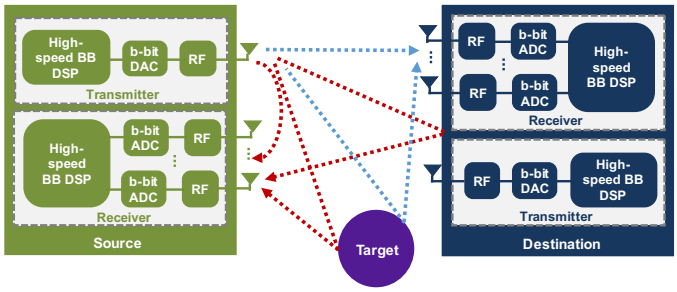

Fig. 1. A full-duplex joint communication-radar scenario, where first a source vehicle sends preamble to the communicating target vehicle, while simultaneously receiving the echoes of the surrounding objects in the presence of self-interference.

uniform linear array (ULA) with M elements and an inter-element spacing of $\leq \frac{\lambda}{2}$, where λ is the carrier wavelength. The JCR transmit and radar RX antennas are assumed to be closely separated such that they will see the same location parameters (e.g., azimuth/elevation angle and range) of a target and aid in providing isolation for full-duplex operation. The single directional TX antenna is assumed to have a notch in its antenna pattern aligned with the end-fire direction, allowing further suppression of direct self-interference due to full-duplex operation. The communication receiver is widely separated from the JCR transmitter.

We consider a single carrier physical layer TX waveform structure with μ fraction of preamble symbols and $1-\mu$ fraction of communication data symbols in a coherent processing interval of T seconds, similar to the mmWave WLAN standard [14] and 5G experimental testbed [12]. We consider the preamble of length N consists of codes that posses good correlation properties for radar detection and communication channel estimation and is denoted by a vector $\mathbf{t}$. Some examples include Zadoff-Chu sequence used in LTE and Golay complementary sequences implemented in 60 GHz WLAN.

The radar channel is assumed to consist of L paths with channel vectors $\mathbf{h}_\ell \in \mathcal{C}^{M\times 1}$ that comprise of line-of-sight (LoS) and non-LoS reflections from near-by objects along with the residual self-interference, as shown in Fig. 1. The circulant-shift matrix of the training sequence vector $\mathbf{t}$ is denoted by $\mathbf{G}^{\mathrm{T}}$, where the ℓ^{th} row of $\mathbf{G}^{\mathrm{T}}$ is obtained by circularly shifting $\mathbf{t}$ by ℓ. Denoting $\mathbf{w}$ as the noise vector, $\mathbf{F}_{\mathrm{M}} \in \mathcal{C}^{M\times M}$ as the DFT matrix, the ℓ^{th} virtual channel coefficient vector $\mathbf{x}_\ell = \mathbf{F}_{\mathrm{M}}\mathbf{h}_\ell$, the virtual channel matrix $\mathbf{X} = [\mathbf{x}_0, \cdots, \mathbf{x}_{\mathrm{L}-1}]$, the complex-baseband received radar signal after discarding the cyclic prefix can be represented as

$$\mathbf{y} = (\mathbf{G}^{\mathrm{T}} \otimes \mathbf{F}_{\mathrm{M}})\mathrm{vec}(\mathbf{X}) + \mathbf{w}. \quad (1)$$

The communication received signal model can be similarly written as (1) with different channel parameters.

III. Measurement JCR Platform

In this section, we describe both the hardware and software platform developed for our mmWave JCR testbed. First, we developed a full-duplex single-input-single-output (SISO) JCR set-up by extending the bi-static NI experimental 5G communication testbed. Then, we extended this set-up for a single-input-multiple-output (SIMO) mmWave JCR channel sounding system.

TABLE I
Hardware Specifications for Our MmWave JCR Testbed

Frequency band	71-76 GHz
Bandwidth (W)	2 GHz
Sampling rate (T_{s})	1.536 GHz
DAC	14 bit with 3.072 GSps
ADC	12 bit with 3.072 GSps
Sliding rail length	21 cm

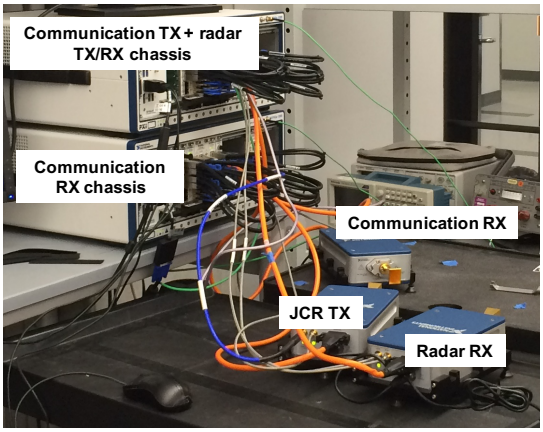

Fig. 2. The mmWave joint communication and radar set-up with mono-static radar and bi-static communication in a SISO configuration. The radar and communication functionalities share a common fully-digital waveform to enable hardware/spectrum reuse. The radar is in a full-duplex mode and the interference between the radar TX and RX depends on the distance between them or the isolation provided by the objects between them.

The mmWave JCR testbed in a (SISO) set-up with 2 GHz bandwidth is shown in Fig. 2. This set-up extends the mmWave communication testbed developed by NI [10] for JCR functionality in a full-duplex configuration. We developed the JCR testbed using two NI PXIe-1085 express chassis. One of the chassis acts as the source JCR that consists of a communication transmitter and radar receiver and the other chassis acts as the destination communication receiver. Each chassis houses NI PXIe-8135 controller, NI PXIe 7902 FPGA for baseband TX/RX processing, NI PXIe 3610 DAC module, NI PXIe 3630 ADC module, and NI PXIe 3630 for IF up-/down-conversion. The IF/LO module is connected to mmWave TX/RX head(s) for up-/down-conversion to 71-76 GHz band and then these mmWave heads are connected to the horn antennas for over-the-air JCR transmission. The two chassis can be synchronized using a Rubidium clock. The specifications for these modules are given in Table I.

We have also synthesized a SIMO testbed by moving the TX antenna on a slider using a stepper motor to collect RX signals with multiple TX-RX inter-spacing for communication and radar receivers simultaneously, as shown in Fig. 3. The inter-distance between any two consecutive TX locations is

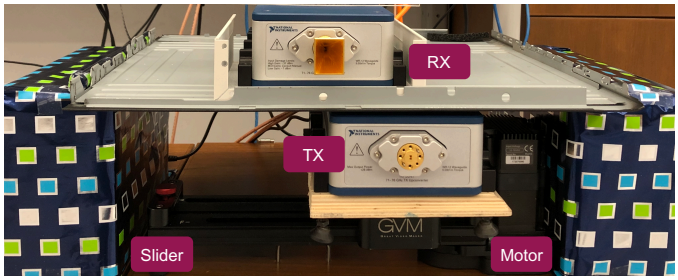

Fig. 3. Sliding motor to simulate multiple antennas with digital RF chains.

Fig. 4. Experimental setup to demonstrate SIMO feasibility.

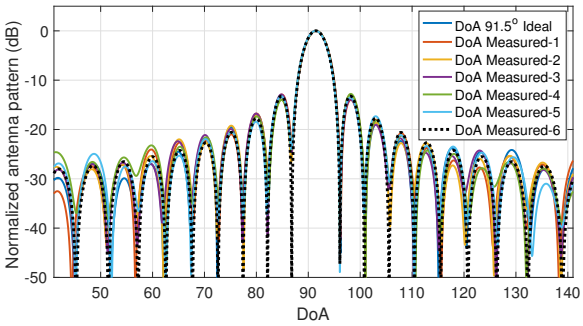

Fig. 5. SIMO antenna pattern obtained corresponding to the corner reflector.

kept less than or equal to half of the carrier wavelength to avoid any grating lobes. The smaller the inter-distance, the better the beamforming shape. The number of locations of the TX on the slider dictates the aperture length of the synthetic antenna, the resolution in the angle domain, and the far-field distance. For each TX location, the transmitter sends several training sequences and then wait to RX echoes for a predefined time interval before moving on to the next step. The time interval between two TX locations is kept large enough to avoid any target range ambiguity. Due to the time-domain channel reciprocity, the channel obtained using multiple TX locations and a fixed RX location will equivalently represent the channel that could have been obtained using multiple RX antenna locations with a fixed TX antenna location. Therefore, moving the JCR transmitter to several locations with fixed RX antennas for radar and communication, we equivalently obtain the SIMO channel for both radar and communication simultaneously. In this paper, we use our mmWave SIMO JCR testbed for static joint communication and radar testing. This testbed, however, can be extended for dynamic scenarios using smaller time intervals between steps and enhanced processing such as used in inverse synthetic aperture radar [15].

Zadoff-Chu training sequences of length 2048 are used in our mmWave JCR testbed. The received raw signal $\mathbf{y}$ from the RX mmWave head of our real-time JCR sounding testbed is used for evaluating the performance of radar offline through emulations. We employ both traditional FFT-based processing and advanced sparse reconstruction using the generalized approximate message passing (GAMP) algorithm with expectation-maximization (EM) and a Bernoulli Gaussian mixture (BG) model assumption of the channel coefficients [16] to estimate the channel in range-angle domain, which corresponds to the virtual channel matrix $\mathbf{X}$ in (1).

IV. Experimental Results

In this section, we describe different experiments conducted using our fully-digital wideband mmWave testbed for the performance evaluation of JCR at 73 GHz. First, we conduct an experiment to demonstrate the SIMO feasibility. Second, we conduct simultaneous radar and communication channel estimation to explore receiver diversity.

To demonstrate the feasibility of the SIMO mode of our developed mmWave JCR testbed, we used an RX horn antenna with 10 dBi gain and a corner reflector of 8.1 cm edge length at a distance of 2.6 m near the boresight, as shown in Fig. 4. The directionality of the horn antenna at RX provides some suppression from the nearby clutter, self-interference due to the full-duplex operation, as well as it increases the gain of the received signal. The number of steps collected is 29 with 1.69 mm spacing, which is less than half of the carrier wavelength of 4.1 mm. Fig. 5 depicts the antenna pattern synthesized using the channel impulse response corresponding to the corner reflector for the six consecutive acquisitions. We can see from Fig. 5 that the resulting antenna patterns are close to the ideal pattern at 91.5 degrees with omnidirectional antenna elements. A similar SIMO antenna pattern is observed for the SIMO communication. The slight deviation from the ideal pattern is due to the phase noise of the NI mmWave hardware or due to the directionality of the horn antenna used at the receiver.

We perform simultaneous communication and a radar channel measurement campaign using the JCR sounding platform at 73 GHz in the same indoor lab as in Fig. 4. Using simulations, [17] had shown that the radar channel estimate can be exploited to reduce the overhead of the communication beam-alignment for analog-beamforming architecture at a different mmWave frequency. We, however, explore the receiver diversity for joint communication and radar system that transmits the same waveform with a fully-digital architecture using real channel measurements. The JCR transmitter and the communication receiver were separated by 1.7 m. We moved

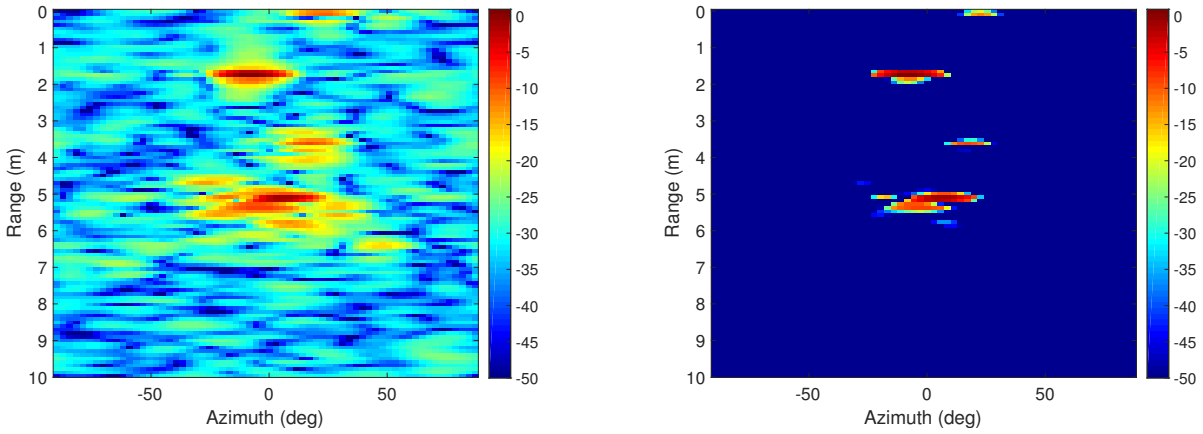

(a) FFT-based (b) GAMP-based

Fig. 6. The radar channel in the range-azimuth domain estimated using the FFT-based processing and the GAMP algorithm with a sparsity constraint. In the radar channel, the full-duplex effect is observed around 0 m along with reflections from surrounding objects, such as the communication receiver at 1.75 m. The channel estimated using GAMP-based processing in (b) detects the full-duplex effect and the surrounding objects with a higher dynamic range than the FFT-based processing in (a).

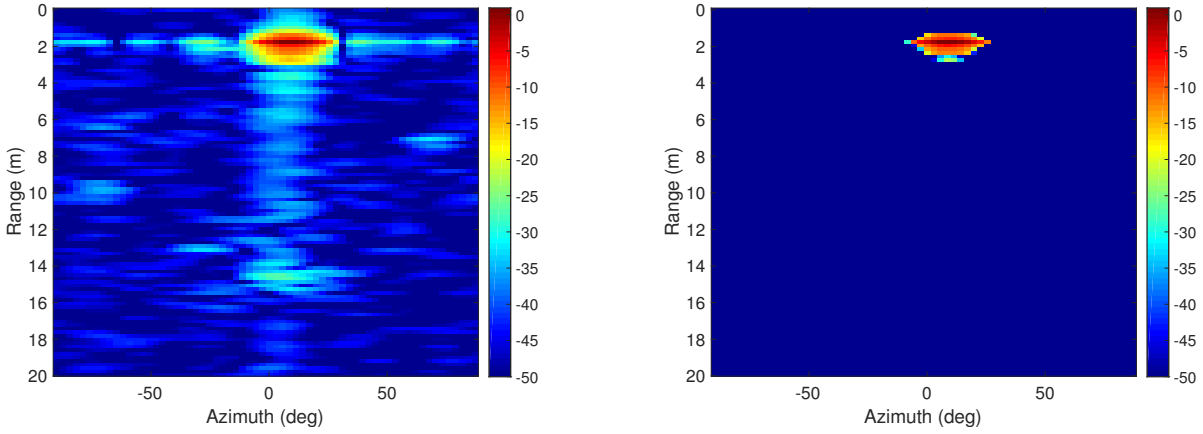

(a) FFT-based (b) GAMP-based

Fig. 7. The communication channel in the range-azimuth domain obtained using the FFT-based processing and the GAMP algorithm with a sparsity constraint. In the communication channel, the LoS path between the communication transmitter and receiver is observed at 1.75 m. The LoS path is much stronger than other reflections suggesting that the mmWave communication channel is LoS-dominated.

the TX with 15 steps on the sliding rail. The radar receiver was located at the same place as the JCR transmitter, as shown in Fig. 3. There was no blockage between the radar and the communication receiver. The directivity of the horn antenna reduced the reflections from the surrounding objects. The wall was behind the communication receiver at 5 m. Between the wall and communication receiver, there was a metallic chassis placed vertically at 3.6 m.

Figs. 6(a) and (b) show the estimated radar channel in the range-azimuth domain using the traditional FFT-based and advanced EM-BG-GAMP processing with a sparsity constraint. We observe the full-duplex effect in the FFT-based radar channel image. We use this full-duplex reference as the zero range reference. We also observe that the direct path corresponding to the communication receiver is at 1.75 m and -8.4 degrees. The wall reflection is more spread as compared to the communication receiver around 4.98 m because of its spatial extent and strong multipath effect due to the large radar cross-section. We also see the reflection of the metallic chassis at 3.613 m. We see that EM-BG-GAMP processed radar image with the sparsity constraint in Fig. 6(b) achieves a higher dynamic range with reduced sidelobes than the FFT-based radar image in Fig. 6(a). The GAMP processing detects the full-duplex effect, communication receiver, as well as the wall without any false detections.

Figs. 7(a) and (b) show the estimated communication channel in the range-azimuth domain using the traditional FFT-based and advanced EM-BG-GAMP processing with a sparsity

constraint. We can see the line of sight (LoS) path between the communication transmitter and receiver at 1.75 m and 8.4 degrees. Other reflections in the communication channel seem much weaker than the line-of-sight channel. This suggests that mmWave channel at small distances without blockage is LoS-dominated.

On comparing Figs. 6(a) and (b) with Figs. 7(a) and (b), we see that the communication receiver is reflected at the same range as the radar, while the azimuth angle is same in magnitude but with opposite sign. This suggests that LoS targets in the two-way radar channel and the LoS path in the one-way communication channel can have a one-to-one relation. For multi-path reflections, however, the relation could be more complex, such as wall reflections. We also observe that sometimes the reflections in the radar channel might not have an equivalent in the communication channel or vice versa. For instance, there is no full-duplex effect observed in the communication channel because our communication receiver is far away from the JCR transmitter as compared to the radar receiver. The delay spread for estimated radar channel in Fig. 6(b) is higher than the communication channel in Fig. 7(b). We also see that there is more multipath near the LoS path between communication receiver and JCR transmitter in the communication image as compared to the radar image. This could be due to the lower path-loss of these multi-path reflections in a one-way bi-static communication channel as compared to the two-way mono-static radar channel. Additionally, the resolution of the radar image is higher than the communication channel due to the two-way path delay instead of the one-way path delay. Therefore, Figs. 6(a) and (b) and Figs. 7(a) and (b) suggest that joint radar and communication channel estimation would improve both radar channel estimate as well as communication channel estimate by taking into account the receiver diversity that results in the similarities and dissimilarities between these channels for LoS path, multi-path, and blockage effects. They also suggest that the radar and communication channel impose a bit different requirements for their joint waveform design.

V. Conclusion

We developed a fully-digital joint communication-radar sounding testbed with SIMO functionality and software-defined architecture at 73 GHz with 2 GHz bandwidth. For the demonstration and evaluation of our SIMO JCR measurement platform, we conducted experiments in the indoor setting and applied both traditional FFT-based and advanced GAMP processing. The results in this paper demonstrate the high-resolution capability with a wide field of view of our low-complexity wideband a fully-digital joint communication-radar testbed. The GAMP processing technique provided enhanced radar and communication channel estimates with a larger dynamic range as compared to the FFT-based processing. The insights in this paper can be taken into account for designing a JCR waveform and developing receive processing for radar and communication with improved performance.

In our future work, we will present low-complexity proof-of-concept development for low-resolution JCR systems at the mmWave band.

Acknowledgment

We would like to thank National Instruments' Wireless Lead User Team for their assistance with the mmWave communication testbed. This material is based upon work supported in part by the National Science Foundation under Grant No. ECCS-1711702 and the U.S. Department of Transportation through the Data-Supported Transportation Operations and Planning (D-STOP) Tier 1 University Transportation Center.

References

[1] J. Choi, V. Va, N. Gonzalez-Prelcic, R. Daniels, C. R. Bhat, and R. W. Heath, "Millimeter-wave vehicular communication to support massive automotive sensing," *IEEE Commun. Mag.*, vol. 54, no. 12, pp. 160–167, December 2016.

[2] J. Lien, N. Gillian, M. E. Karagozler, P. Amihood, C. Schwesig, E. Olson, H. Raja, and I. Poupyrev, "Soli: Ubiquitous gesture sensing with millimeter wave radar," *ACM Trans. on Graphics (TOG)*, vol. 35, no. 4, p. 142, 2016.

[3] K. V. Mishra, M. R. Bhavani Shankar, V. Koivunen, B. Ottersten, and S. A. Vorobyov, "Toward millimeter-wave joint radar communications: A signal processing perspective," *IEEE Signal Process. Mag.*, vol. 36, no. 5, pp. 100–114, Sep. 2019.

[4] P. Kumari, N. Gonzalez-Prelcic, and R. W. Heath Jr, "Investigating the IEEE 802.11ad Standard for Millimeter Wave Automotive Radar," in *Proc. IEEE Veh. Technol. Conf.*, September 2015, pp. 3587–3591.

[5] P. Kumari, J. Choi, N. González-Prelcic, and R. W. Heath, "IEEE 802.11ad-based radar: An approach to joint vehicular communication-radar system," *IEEE Trans. Veh. Technol.*, vol. 67, no. 4, pp. 3012–3027, April 2018.

[6] E. Grossi, M. Lops, L. Venturino, and A. Zappone, "Opportunistic radar in IEEE 802.11ad networks," *IEEE Trans. Signal Process.*, vol. 66, no. 9, pp. 2441–2454, May 2018.

[7] P. Kumari, M. E. Eltayeb, and R. W. Heath, "Sparsity-aware adaptive beamforming design for IEEE 802.11ad-based joint communication-radar," in *Proc. IEEE Radar Conf.*, April 2018, pp. 0923–0928.

[8] W. Kim, "Experimental demonstration of mmwave vehicle-to-vehicle communications using IEEE 802.11ad," *Sensors*, vol. 19, no. 9, 2019. [Online]. Available: https://www.mdpi.com/1424-8220/19/9/2057

[9] H. Ajorloo, C. J. Sreenan, A. Loch, and J. Widmer, "On the feasibility of using IEEE 802.11ad mmwave for accurate object detection," in *Proc. of the ACM/SIGAPP Symposium on Applied Computing*, ser. SAC '19. New York, NY, USA: ACM, 2019, pp. 2406–2413.

[10] NI mmWave transceiver system. [Online]. Available: http://www.ni.com/sdr/mmwave/

[11] T. S. Rappaport, J. R.W. Heath, J. N. Murdock, and R. C. Daniels, *Millimeter Wave Wireless Communications*. Pearson, 2014.

[12] M. Cudak, T. Kovarik, T. A. Thomas, A. Ghosh, Y. Kishiyama, and T. Nakamura, "Experimental mm wave 5G cellular system," in *Proc. IEEE Globecom Workshops*, Dec 2014, pp. 377–381.

[13] R. Gomes, L. Sismeiro, C. Ribeiro, T. R. Fernandes, M. G. Sanchéz, A. Hammoudeh, and R. F. S. Caldeirinha, "Will COTS RF front-ends really cope with 5G requirements at mmWave?" *IEEE Access*, vol. 6, pp. 38 745–38 769, 2018.

[14] "Wireless LAN Medium Access Control (MAC) and Physical Layer (PHY) Specifications. Amendment 3: Enhancements for Very High Throughput in the 60 GHz Band," *IEEE Std. 802.11ad*, 2012.

[15] C. Ozdemir, *Inverse synthetic aperture radar imaging with MATLAB algorithms*. John Wiley & Sons, 2012, vol. 210.

[16] J. P. Vila and P. Schniter, "Expectation-maximization Gaussian-mixture approximate message passing," *IEEE Trans. on Signal Process.*, vol. 61, no. 19, pp. 4658–4672, Oct 2013.

[17] N. González-Prelcic, R. Méndez-Rial, and R. W. Heath, "Radar aided beam alignment in mmWave V2I communications supporting antenna diversity," in *Proc. Information Theory and Applications Workshop*, Jan 2016, pp. 1–7.